EFFECT OF ASSUMED DAMAGE AND LOCATION ON THE DELAMINATION ONSET PREDICTIONS FOR SKIN-STIFFENER DEBONDING

Isabelle L. Paris
National Research Council Research Associate
NASA Langley Research Center
Hampton, Virginia

Ronald Krueger
ICASE Staff Scientist
NASA Langley Research Center
Hampton, Virginia

T. Kevin O'Brien
Senior Scientist
U.S. Army Research Laboratory, Vehicle Technology Directorate,
NASA Langley Research Center
Hampton, Virginia

ABSTRACT

The difference in delamination onset predictions based on the type and location of the assumed initial damage are compared in a specimen consisting of a tapered flange laminate bonded to a skin laminate. From previous experimental work, the damage was identified to consist of a matrix crack in the top skin layer followed by a delamination between the top and second skin layer (+45º/-45º interface). Two-dimensional finite elements analyses were performed for three different assumed flaws and the results show a considerable reduction in critical load if an initial delamination is assumed to be present, both under tension and bending loads. For a crack length corresponding to the peak in the strain energy release rate, the delamination onset load for an assumed initial flaw in the bondline is slightly higher than the critical load for delamination onset from an assumed skin matrix crack, both under tension and bending loads. As a result, assuming an initial flaw in the bondline is simpler while providing a critical load relatively close to the real case. For the configuration studied, a small delamination might form at a lower tension load than the critical load calculated for a 12.7 mm (0.5") delamination, but it would grow in a stable manner. For the bending case, assuming an initial flaw of 12.7 mm (0.5") is conservative, the crack would grow unstably.

INTRODUCTION

This study focused on skin-stiffener debonding resulting from buckling of a thin-gage composite fuselage structure. The case study presented here was undertaken to illustrate the difference in delamination onset predictions based on the type and location of the

assumed initial damage. The goal is to extend these comparisons to a more classical damage tolerance approach assuming delamination from a critical size initial flaw at the most critical location.

In an earlier study [1], it was found that typical stiffener pull-off specimens yielded the same failure mode as a smaller and simpler specimen consisting of a tapered flange laminate bonded to a skin laminate (Figure 1). Two damage patterns were observed experimentally at the flange tip [2]. However, the first damage occurring experimentally was delamination at corners 2 and 3, where a matrix crack forms in the 45º skin surface ply and creates a delamination at the +45º/-45º interface (Figure 2 (a)). Therefore, this damage pattern was the focus of the model. Design curves were developed for skin-stiffener debonding for a given stiffener flange/skin layup and geometry in terms of critical values for membrane and bending resultants at the flange tip [3]. These curves were obtained for the onset of first failure in a virgin, as-designed, configuration.

BACKGROUND

The specimen configuration, material and loading cases selected in this case study have been the subject of a previous experimental work. A summary of the experiments is provided here and more details can be found in reference [2].

Materials

The specimens consisted of a tapered laminate, representing the stringer flange, bonded onto a skin as shown in Figure 1. An IM7/8552 graphite/epoxy system was used for both the skin and flange. The skin was made of prepreg tape and had a nominal ply thickness of 0.142 mm (0.0056”) and a [45/-45/0/-45/45/90/90/-45/45/0/45/-45] lay-up. The flange was made of a plain-weave fabric of 0.208 mm (0.0082”) nominal ply thickness. The flange lay-up was $[45/0/45/0/45/0/45/0/45]_f$, where the subscript “f” denotes fabric, “0” represents a 0°-90° fabric ply and “45” represents a 0°-90° fabric ply rotated by 45º.

The flange was pre-cured, cut to size, machined with a 25° taper along the edges and co-bonded with the uncured skin using one ply of grade 5, FM300 adhesive film. A diamond saw was used to cut the panels into 25.4-mm (1”) -wide by 177.8-mm (7”) -long specimens. The average ply thickness obtained from specimen thickness measurements and micrographs was 0.148 mm (0.0058”) for the tape, 0.212 mm (0.0083”) for the fabric and 0.178 mm (0.007”) for the adhesive. The properties of the graphite/epoxy material and the adhesive were measured at Boeing and are part of the standard design database for the V-22 tilt-rotor aircraft. Typical properties are summarized in Table I.

Experimental procedure

Quasi-static tension tests were performed in a servohydraulic load frame in displacement control at a stroke rate of 0.4 mm/min (0.016 in/min). The specimens were mounted in hydraulic grips with a gage length of 101.6 mm (4”). A total of 4 specimens were tested. An extensometer with a 25.4 mm (1”) gage length was mounted on the backside of the specimen and centered on the flange tip. A damage onset load was determined at which a small initial load drop was observed prior to flange debonding.

The value of the damage onset load was averaged from four tests and determined to be 17.8 kN (4 kips) which was later designated as P_{crit}. The tests were terminated when the flange debonded from the skin.

The 3-point bending tests were also run in a servohydraulic load frame at a monotonic rate of 1.52 mm/min (0.06 in/min). The bottom support had a 101.6 mm (4") span. Mid-span deflections were recorded using a spring loaded direct current displacement transducer (DCDT) contacting the center of the flange. A damage onset load was determined at which a small initial load drop was observed prior to flange debonding. The value of the damage onset load was averaged from four tests and determined to be 427.6 kN (96.1 kips) which was later designated as P_{crit}. The tests were stopped after the flange had debonded from the skin.

ANALYTICAL INVESTIGATION

The first analytical model (Case 1 in Figure 2) represented the actual failure pattern observed in the experiment. This consisted of a matrix crack in the skin surface layer followed by a delamination at the +45º/-45º interface. Although this case is the most realistic, it is more difficult to model. Also, if an experimental validation is wanted, it is more difficult to manufacture a specimen with an embedded flaw that simulates both the delamination and the matrix crack. In the second model (Case 2) a flaw was assumed to exist in the bondline, creating a delamination, as shown in Figure 2. This case would be the easiest to simulate experimentally and would simplify modeling, but the approach is different from the actual situation where the delamination occurs at a ply interface within the skin. In the third case, (Case 3) a delamination was assumed at the +45º/-45º interface without the matrix crack. Although the delamination is located at the correct interface, the approach is simplified by the absence of the matrix crack. However, the absence of the matrix crack might change the response of the specimen. The goal of this investigation was to verify if the simplifications made in cases 2 and 3 are conservative.

A two-dimensional, plane stress finite element model was utilized which closely approximates the specimen geometry, boundary conditions and the two loading conditions applied during the tests. It is inherent to a two dimensional FE model that the geometry, boundary conditions and other properties are constant across the entire width of the model. This may not always capture the true nature of the problem. As shown in reference [2], the delamination pattern changed from corner 3 to corner 4 from a delamination running in the 45°/-45° interface to a delamination propagating in the bondline. These three-dimensional patterns of matrix cracks and delaminations, which vary across the width of the specimen, can not be accounted for in any two-dimensional FE model. In addition, the plane-stress model imposes $\sigma_{zz}=\tau_{xz}=\tau_{yz}=0$ at the free edge of each ply and allows the displacement to be the free parameter. The plane-strain model, on the other hand, imposes $\varepsilon_{zz}=\gamma_{xz}=\gamma_{yz}=0$ at the free edge, which excessively constrains the plies. An alternative to a full three-dimensional simulation might be a generalized plane-strain model, which requires about the same modeling effort as a simple two-dimensional model. The generalized plane-strain case may be regarded as an intermediate state, and it is assumed that $\varepsilon_{zz}=-\nu_L\varepsilon_{xx}$ and $\gamma_{xz}=\gamma_{yz}=0$ where ν_L is the laminate Poisson's ratio. The current study, however, was restricted to the use of two-dimensional models because industry requires fast and simple simulations. A plane stress model was preferred for this

study due to the constraints inherent to the plane-strain model, particularly in the ±45° plies as discussed in [2]. Moreover, since the goal of the present study is to compare the damage onset prediction for different damage location and type (case 1, 2 and 3), the relative difference between those predictions should be marginally affected by the plane stress assumption. A comparison of two-dimensional FE modeling versus detailed three-dimensional analysis for this specimen configuration is given in [4].

The schematics of the model of the specimen, boundary conditions, and loads applied are shown in Figure 3. The model was analyzed using the geometrically nonlinear solution option in the ABAQUS® finite element code. Eight-noded quadrilateral plane-stress (CPS8R) elements with quadratic shape functions and a reduced (2x2) integration scheme were utilized for the geometric non-linear analyses. Some six-noded triangular elements were used in the tapered edge. A refined mesh was used in the critical areas where delaminations were modeled. Detailed views of the mesh can be seen in Figure 4. Outside the mesh refinement areas, all plies were modeled with one element through the ply thickness. In the refined regions, four elements were used per ply thickness. Typical ply properties and adhesive material properties are summarized in Table I.

Damage was modeled by discrete discontinuities, which means that the elements above and below the delamination are not connected, as shown in Figure 4. The goal was to increase the delamination length up to 12.7 mm (0.5”), which corresponds to the smallest delamination size that could be detected by ultrasonic inspection. Smaller defects would be more difficult to detect because of the change in thickness in the tapered region. Opening and shear strain energy release rate components, G_I and G_{II}, were calculated using the Virtual Crack Closure Technique (VCCT), as described in reference [4]. The total strain energy release rate G_T was obtained by summing the individual mode components.

Tension load

First, a tension load equal to the experimentally measured critical load to form the first matrix crack in the 45º skin ply was applied to the specimen and the total strain energy release rate, G_T, versus delamination length curve was generated (Figure 5). For all three cases, the total strain energy release rate increases with crack length and reaches a peak around the beginning of the first flange ply, indicated by the dotted line B. The peak G_T is the highest for case 1, the actual matrix crack and delamination in the +45º/-45º interface, and is lower for the bondline flaw (case 2) and even lower for the +45º/-45º interface delamination with no matrix crack (case 3). For case 3, the analysis was only performed up to 7.9 mm (0.31 in) delamination length, since crack face contact was observed at longer delamination lengths.

The mixed mode rate is characterized by the proportion of mode II, G_{II}/G_T, as shown in Figure 6. For all three cases, this ratio decreases, then increases with increasing delamination length. The minimum mode II (maximum mode I) occurs around the beginning of the first flange ply, indicated by the dotted line B. G_{II}/G_T reaches a plateau at the end of the taper (dotted line C). Case 3 has a much higher proportion of mode II at longer crack lengths, with the mode II contribution increasing to 100% for a delamination of 7.9 mm (0.31”), when crack face contact begins.

For a given crack length, the mixed mode-ratio was compared to the mixed-mode delamination criteria curve in Figure 7 [6] to obtain the critical strain energy release rate

G_c. On this curve, the pure mode I case corresponds to the left axis and the pure mode II case corresponds to the right axis. Mixed mode I and II cases are in between. The data is fit using a least square regression to obtain the exponential curve shown. Using this fit, G_c can be determined for a given mixed mode ratio. Then G_T from Figure 5 normalized by this G_c was plotted as a function of delamination length (Figure 8). Although Case 2 is assumed to occur in the bondline, delamination failure criteria (Figure 7) are being used in this case instead of adhesive debonding criteria. Because interlaminar properties are more brittle and interlaminar bond lines are thinner than adhesive bonds, this yields a conservative representation of the actual failure mode in the skin laminate. For all three cases, the total strain energy release rate increases with crack length, reaches a peak value at the beginning of the first flange ply (dotted line B) and then decreases. It stabilizes at the end of the taper (dotted line C). The peak G_T is the highest for Case 1, the actual matrix crack and delamination at the +45º/-45º interface, and is lower for the bondline flaw (Case 2) and even lower for the +45º/-45º interface delamination with no matrix crack (Case 3).

All three cases indicate that G_T calculated at the measured load P_{crit} required to form the matrix crack in the 45º skin surface ply is much larger than G_c ($G_T/G_c>1$). Hence, at this load, the delamination grows immediately once the matrix crack forms. However, to apply a damage tolerance approach assuming an initial flaw, the curves need to be reduced to peak values of G_T equals G_c ($G_T/G_c=1$) to obtain the critical load (P_c) to form a delamination with a pre-existing flaw. Nonlinear analyses for several applied load levels have been performed previously for case 1 [2], which showed a linear relationship between the applied load and the square root of the strain energy release. Therefore P_c was determined as follow:

$$P_c = \sqrt{\frac{G_c}{G_T}} P_{crit}$$

Comparison at the minimum P_c (corresponding to the peak G_T/G_c) illustrates the effect of assumed initial damage type and location (Figure 9). For case 1, the load required to initiate matrix cracking in the 45º skin surface ply is 3 times greater than the load necessary for delamination onset from an assumed matrix crack. Therefore, there is a considerable reduction in critical load if the initial delamination is assumed to be present. The delamination onset load for an assumed initial flaw in the bondline (case 2) is slightly higher (8%) than the critical load for delamination onset from an assumed skin matrix crack (case 1). The critical load for delamination onset in case 3 is even higher (35%), and hence, less conservative, than for case 1 or 2.

An assumed initial flaw of 12.7 mm (0.5”) corresponds to the critical delamination size easily detected by ultrasonic inspection. Under a tension load (Figure 8), the G_T/G_c curve is decreasing with crack length after the peak. This indicates that a delamination would grow stably after it is initiated. Since the G_T/G_c for a delamination of 12.7 mm (0.5”) is lower than the peak G_T/G_c, a small delamination might form at a lower load than the P_c calculated for a 12.7 mm (0.5”) delamination, but it would grow in a stable manner. The difference in critical loads P_c is illustrated in Figure 10 (case 3 is not included on the figure since the calculations were not performed up to 12.7 mm (0.5”) due to crack face contact). The critical load P_c to grow the delamination would still be lower than the load required to initiate the matrix crack.

Bending loads

This study was repeated for an applied bending load. The mixed-mode ratio, (G_{II}/G_T) versus delamination length curves are similar to the tension loading case. For a given crack length, a mixed mode-ratio was obtained and compared to the mixed-mode delamination criteria to obtain a G_c. Then G_T normalized by this G_c was plotted as a function of delamination length (Figure 11). Unlike the tension loading case, these G_T/G_c versus a curves are continuously increasing, indicating unstable delamination growth. The dotted line B indicates the delamination length corresponding to the first fabric flange ply. Because this represents the first point of stiffness discontinuity, and corresponds to the peak in the normalized G_T vs. a curves for the tension loading, critical loads for the three cases were compared at this point (Figure 12). For case 1, the gray bar shows the load required to initiate matrix cracking in the top 45º skin ply while the black bar shows the load necessary for delamination onset from an assumed matrix crack. As was noted earlier for the tension loading, there is a considerable reduction in critical load if the initial delamination is assumed to be present. The delamination onset load for an assumed initial flaw in the bondline is slightly higher (7%) than the critical load for delamination onset from an assumed skin matrix crack (case 1). Recall that delamination failure criteria (Figure 7) are being used for case 2 instead of adhesive debonding criteria. The critical load for delamination onset in case 3 for the +45º/-45º interface delamination without the matrix crack is even higher (36%), and hence, less conservative, than case 1 or 2.

For a bending load, the G_T/G_c curves are constantly increasing for cases 1 and 2 (Figure 10). Therefore, a flaw of 12.7 mm (0.5”) would be more conservative than choosing a G value at the flange tip (stiffness discontinuity), as shown in Figure 13. However, once a delamination forms, it will grow in an unstable manner. Therefore the bending case is more critical than the tension one.

CONCLUSIONS

For the skin/flange specimen configuration studied, it was found that there is a considerable reduction in critical load if the initial delamination is assumed to be present, both under tension and bending loads.

For both loading conditions, using the location where the peak occurs in the G_T/G_c curve, the delamination onset load for an assumed initial flaw in the bondline is slightly higher than the critical load for delamination onset from an assumed skin matrix crack. In the case of an assumed flaw in the +45º/-45º interface without a skin matrix crack, the delamination onset load is even higher. As a result, assuming an initial flaw in the bondline is simpler while providing a critical load relatively close to the real case.

For the tension load and the configuration studied, the G_t/G_c curves decreases with crack length. Therefore, a small delamination might form at a lower load than the P_c calculated for a 12.7 mm (0.5”) delamination, but it would grow in a stable manner. For the bending case however, assuming an initial flaw of 12.7 mm (0.5”) is conservative, but the crack would grow unstably. These results are valid for the configuration studied, and might not hold for a different configuration.

ACKNOWLEDGMENTS

This work was performed as part of a Cooperative Research and Development Agreement (CRDA) between the U.S. Army Research Laboratory, Vehicle Technology Directorate, located at NASA Langley Research Center, and the Boeing Company, Philadelphia, PA.

REFERENCES

1) Minguet, P.J. and O'Brien, T.K., "Analysis of Test Methods for Characterizing Skin/Stringer Debonding Failures in Reinforced Composite Panels," *Composite Materials: Testing and Design*, Twelfth Volume, ASTM STP 1274, August 1996, pp. 105-124.

2) Krueger, R., Paris, I.L. and O'Brien, T.K., "Fatigue Life Methodology for Bonded Composite Skin/Stringer Configurations," Proceedings of the American Society for Composites, Fifteenth Technical Conference, Technomic Publishing, 2000, pp. 729-736 .

3) Krueger, R., Cvitkovich, M.K., O'Brien, T.K. and Minguet, P.J., "Testing and Analysis of Composite Skin/Stringer Debonding under Multi-Axial Loading," *Journal of Composite Materials*, Vol. 34, 2000, pp. 1263-1300.

4) Krueger, R., Paris, I. L., O'Brien, T. K., and Minguet, P. J.,"Effect Of Finite Element Modeling On The Delamination Onset Predictions For Skin-Stiffener Debonding," to be presented at ICCS-11, Melbourne, Australia, November 2001.

5) Raju, I.S., "Calculation Of Strain-Energy Release Rates With Higher Order And Singular Finite Elements," *Eng. Fracture Mech.*, vol. 28, 1987, pp. 251-274.

6) P. Hansen and R. Martin, "DCB, 4ENF and MMB Delamination Characterisation of S2/8552 and IM7/8552," Materials Engineering Research Laboratory Ltd. (MERL), Hertford, U.K., N68171-98-M-5177, 1999.

TABLE 1. MATERIAL PROPERTIES

IM7/8552 Unidirectional Graphite/Epoxy Prepreg		
E_{11} = 161.0 GPa	E_{22} = 11.38 GPa	E_{33} = 11.38 GPa
ν_{12} = 0.32	ν_{13} = 0.32	ν_{23} = 0.45
G_{12} = 5.17 GPa	G_{13} = 5.17 GPa	G_{23} = 3.92 GPa
IM7/8552 Graphite/Epoxy Plain Weave Fabric		
E_{11} = 71.7 GPa	E_{22} = 71.7 GPa	E_{33} = 10.3 GPa
ν_{12} = 0.04	ν_{13} = 0.35	ν_{23} = 0.35
G_{12} = 4.48 GPa	G_{13} = 4.14 GPa	G_{23} = 4.14 GPa
Grade 5 FM300 Adhesive		
E = 1.72 GPa	ν = 0.3	(assumed isotropic)

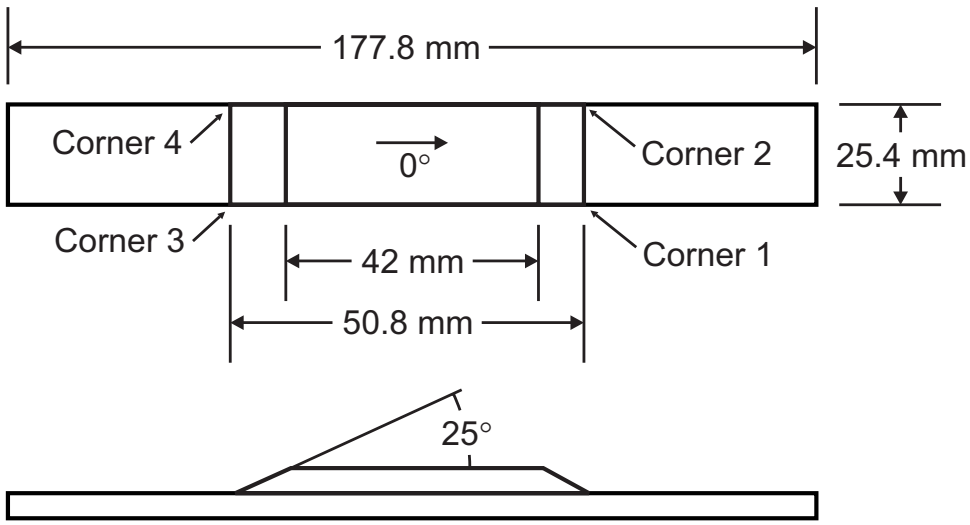

Figure 1. Specimen configuration.

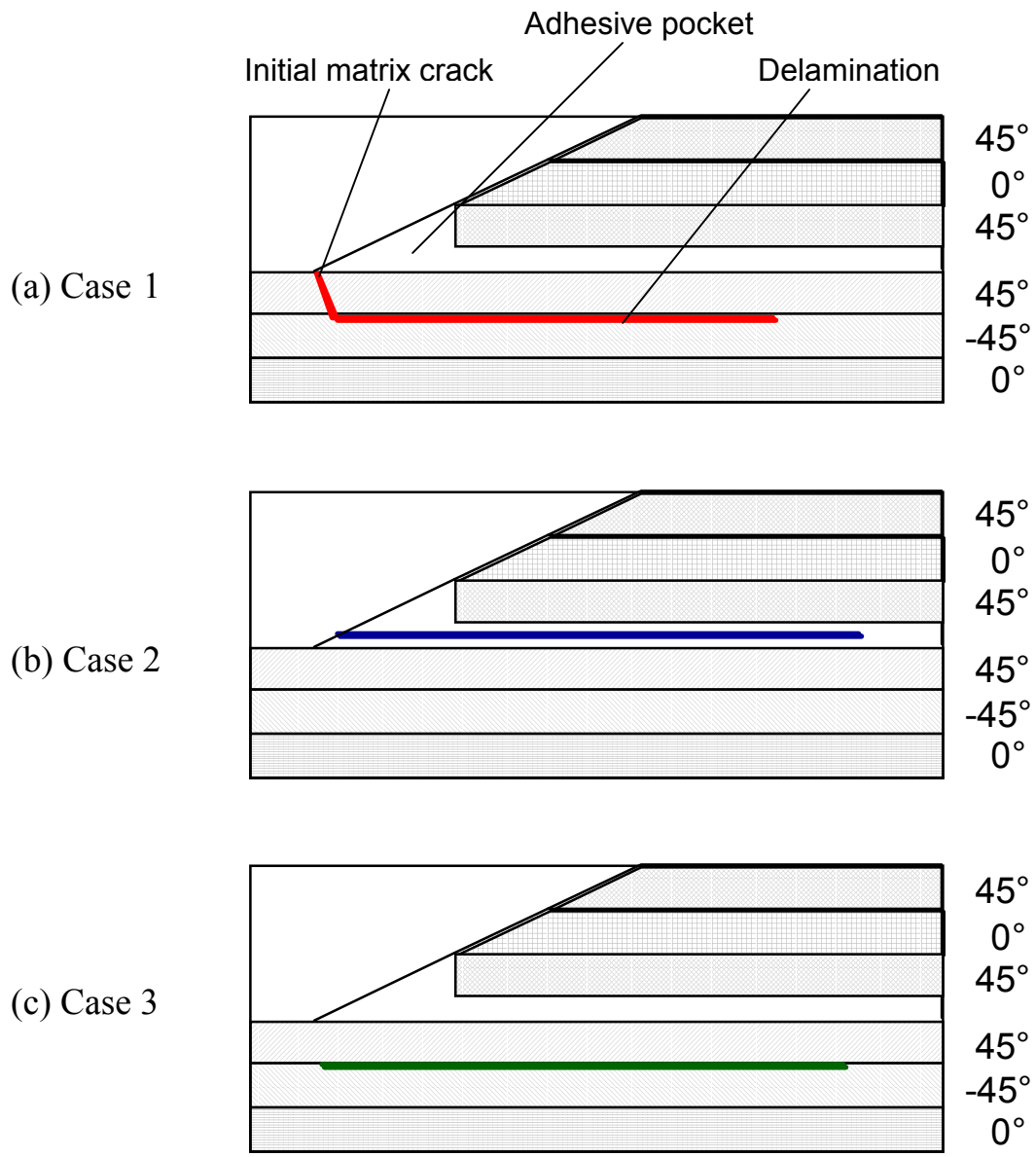

Figure 2. Flaw type and location.

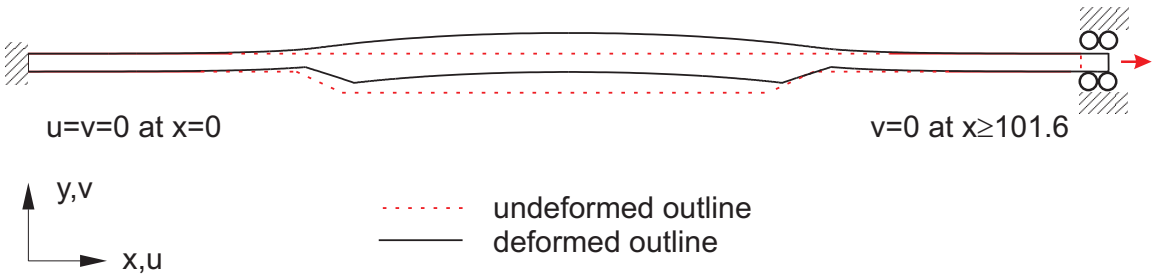

(a) Tension loading

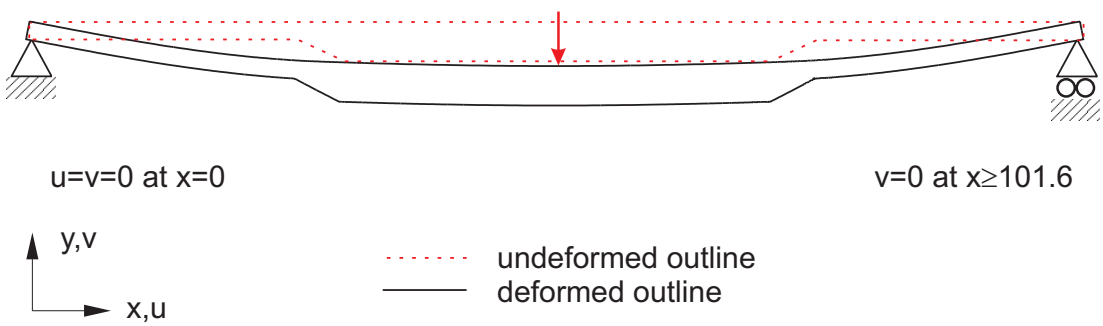

(b) Bending loading

Figure 3. Deformed outline of modeled skin/flange specimen.

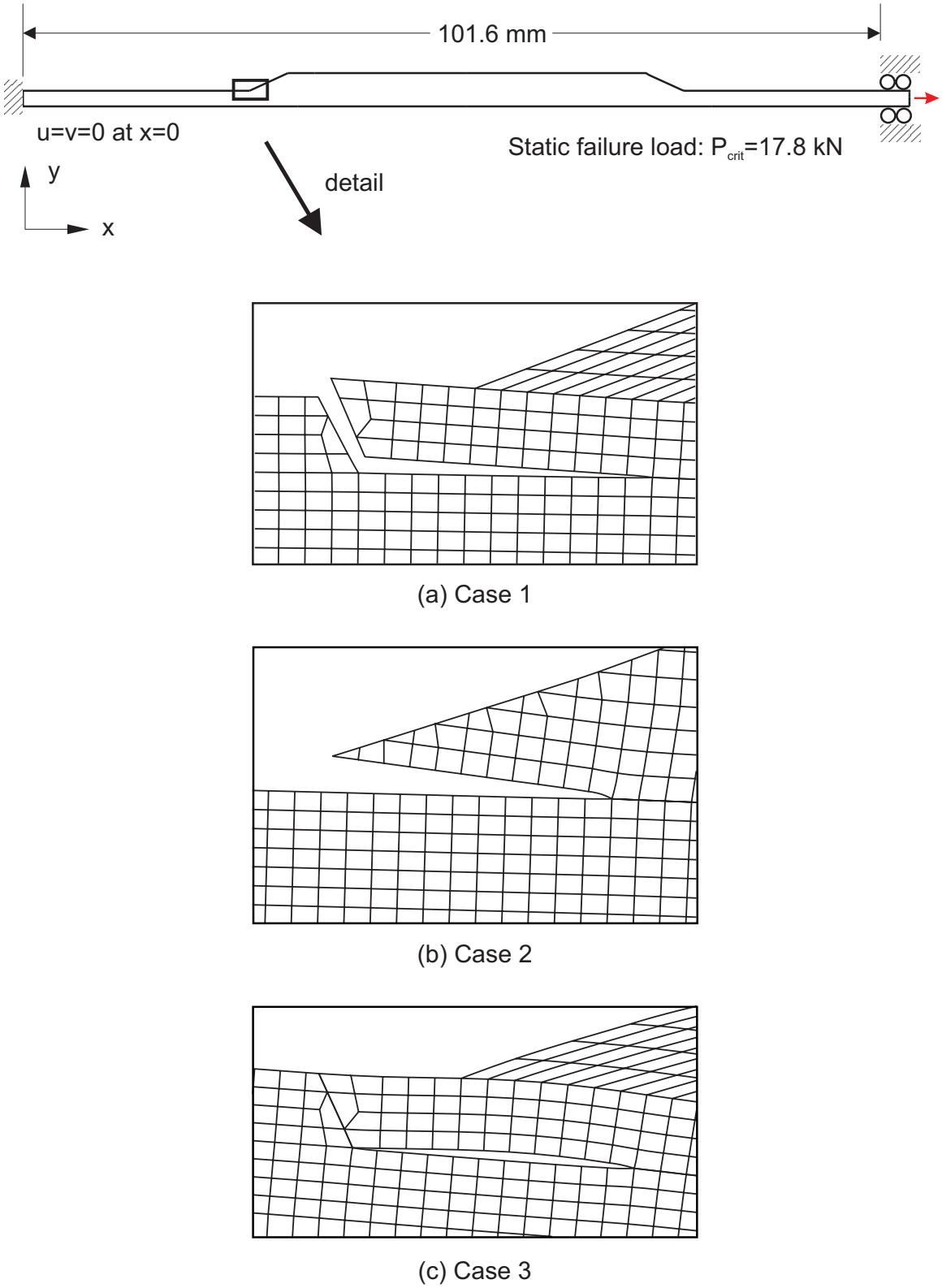

Figure 4. Finite element model of skin/flange specimen.

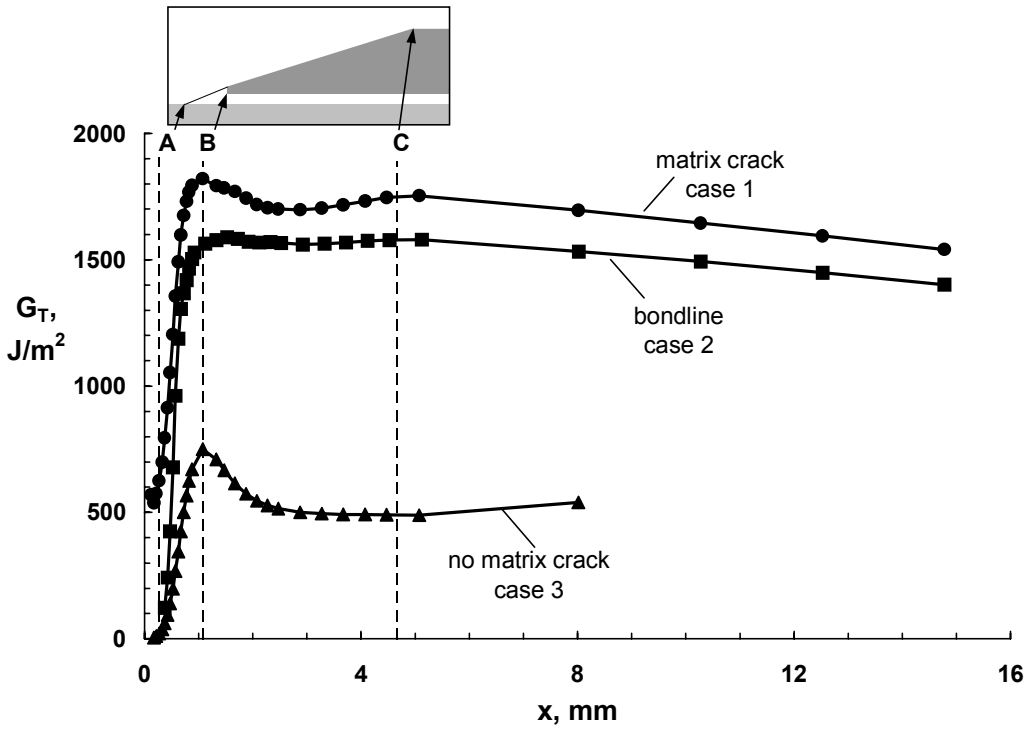

Figure 5. G_T as a function of delamination length for tension loading (x is the distance from the matrix crack); P_{crit}=17.8 kN.

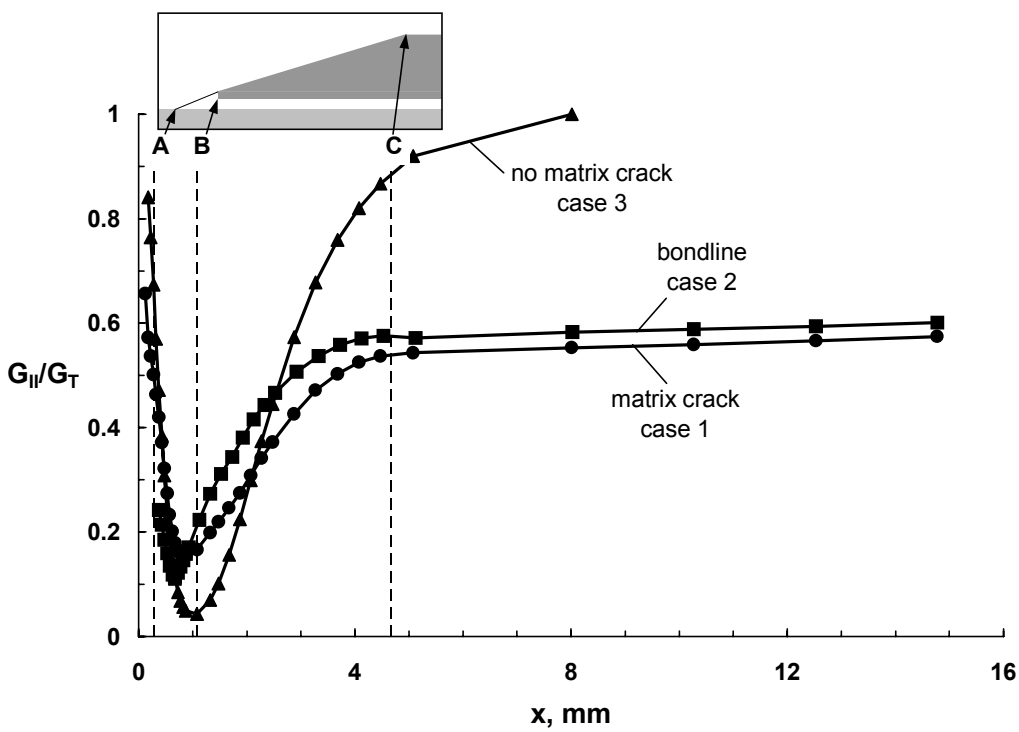

Figure 6. Mixed mode ratio as a function of delamination length for tension loading (x is the distance from the matrix crack) ; P_{crit}=17.8 kN.

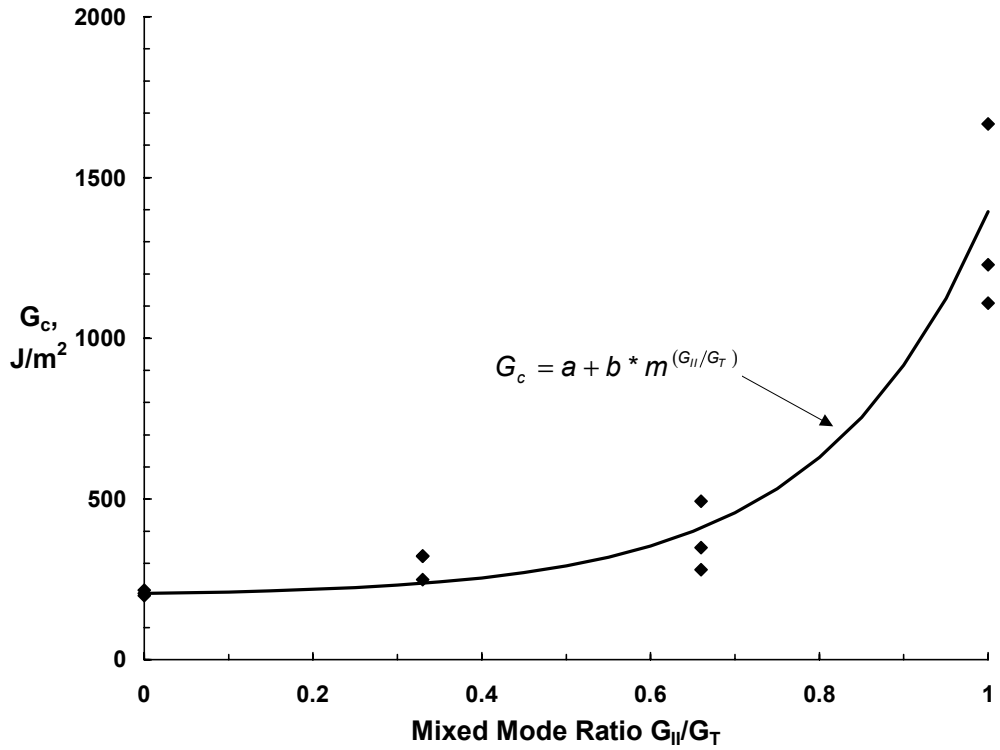

Figure 7. Mixed mode delamination criterion for IM7/8552 [7].

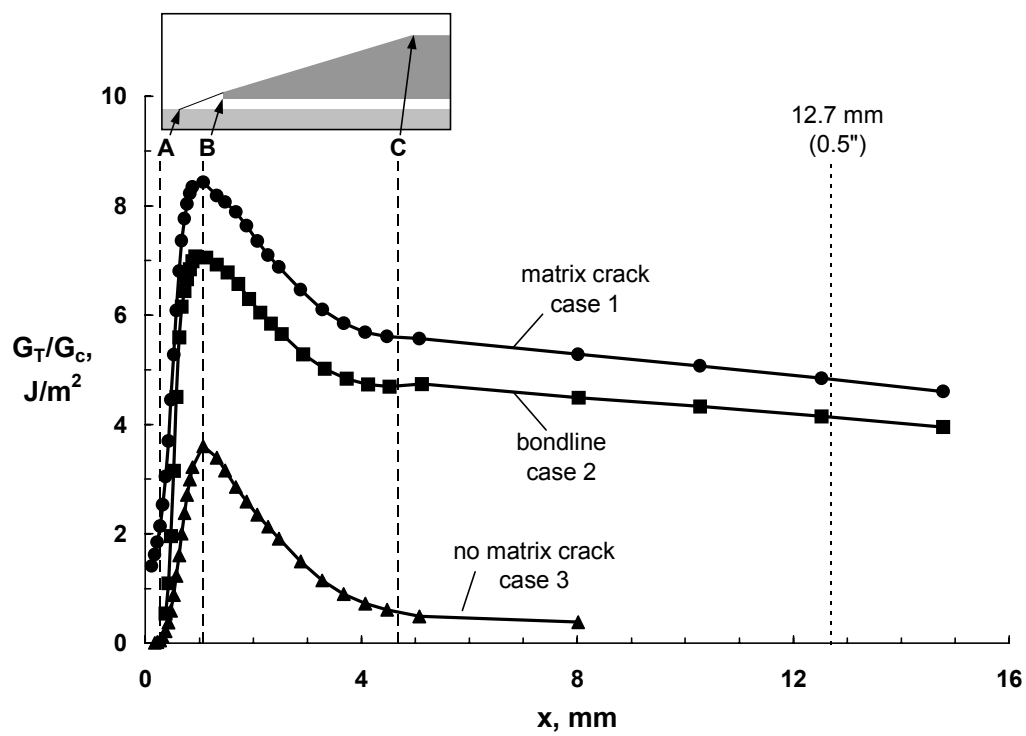

Figure 8. G_T/G_c as a function of delamination length for tension loading (x is the distance from the matrix crack); P_{crit}=17.8 kN.

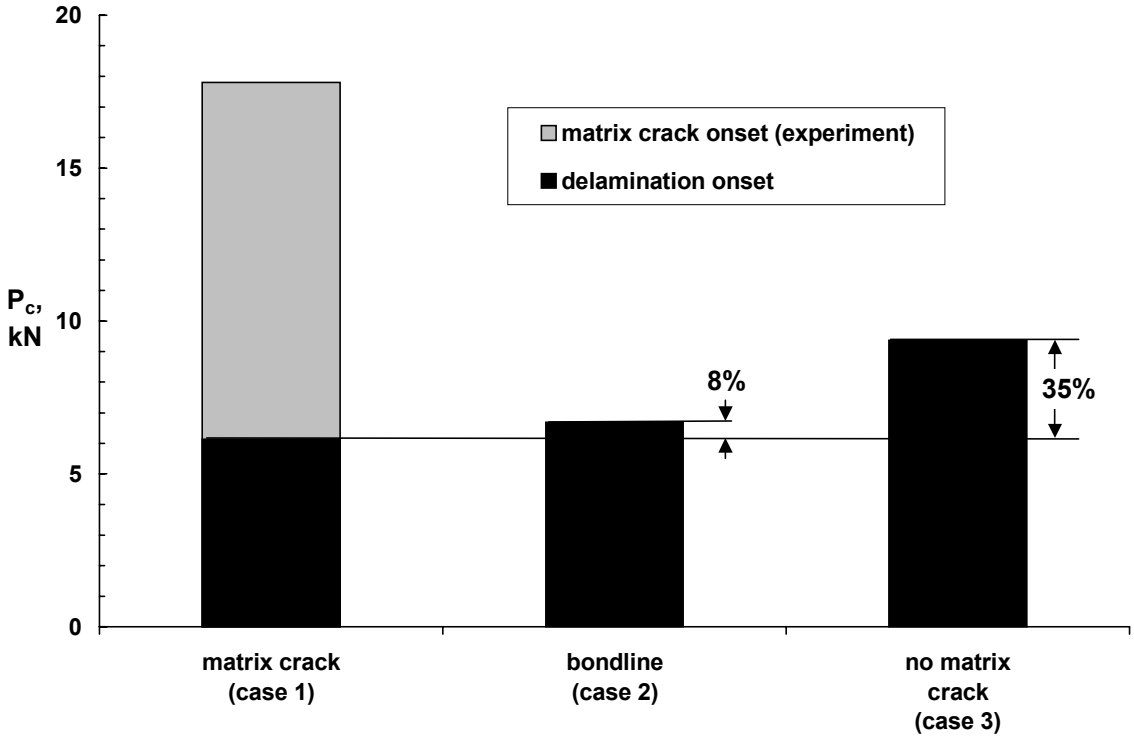

Figure 9. Critical load P_c for tension loading condition.

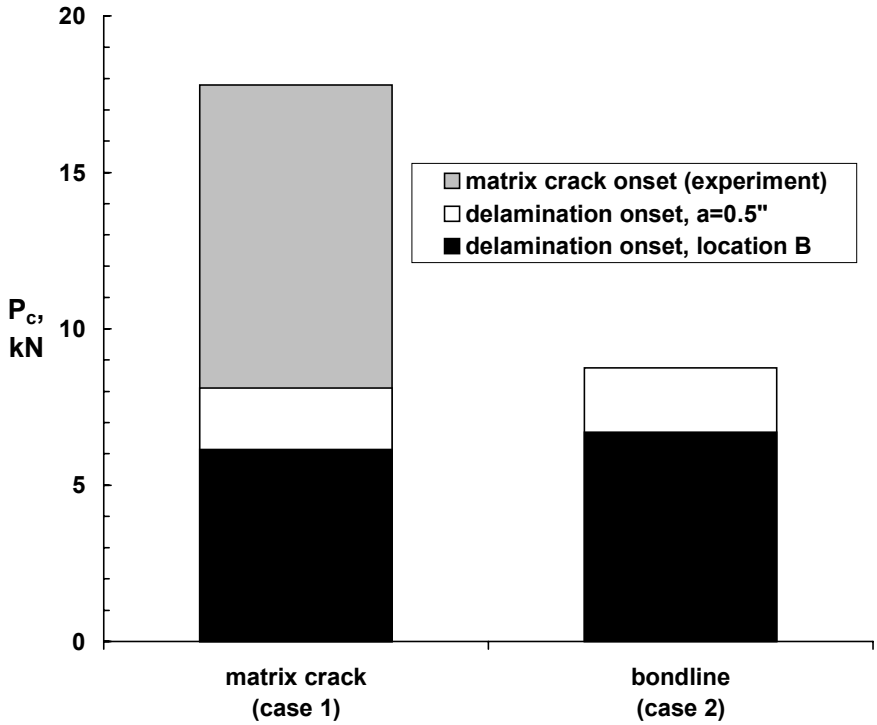

Figure 10. Critical load P_c for an assumed flaw of 12.7 mm (0.5”) for tension loading condition.

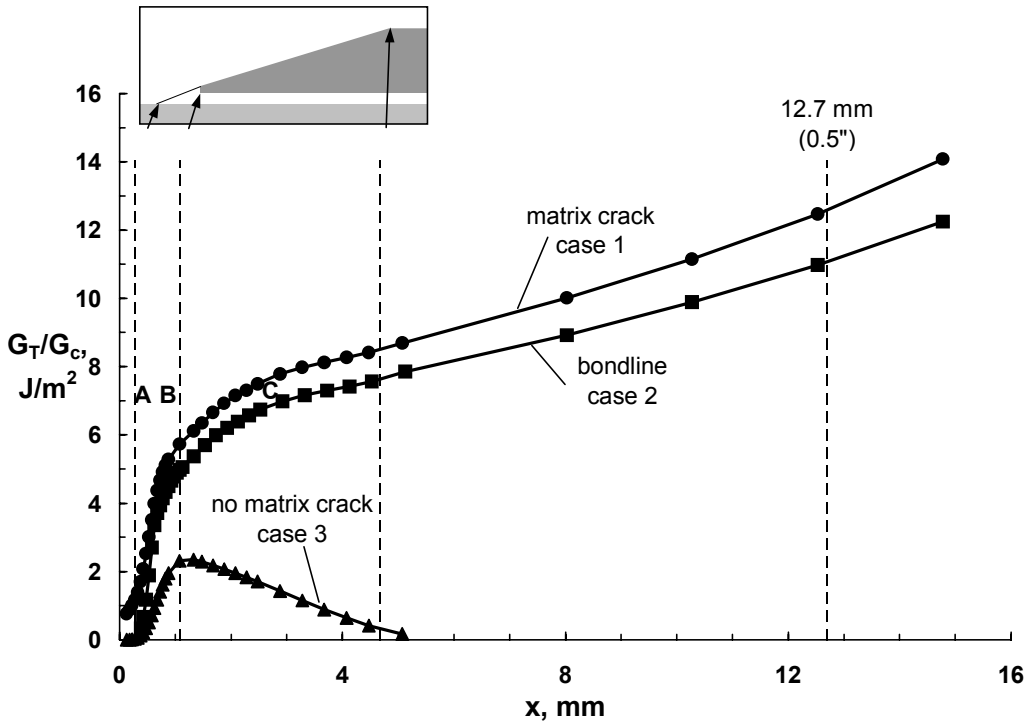

Figure 11. G_T/G_c as a function of delamination length for bending loading (x is the distance from the matrix crack)); P_{crit}=427.6 kN.

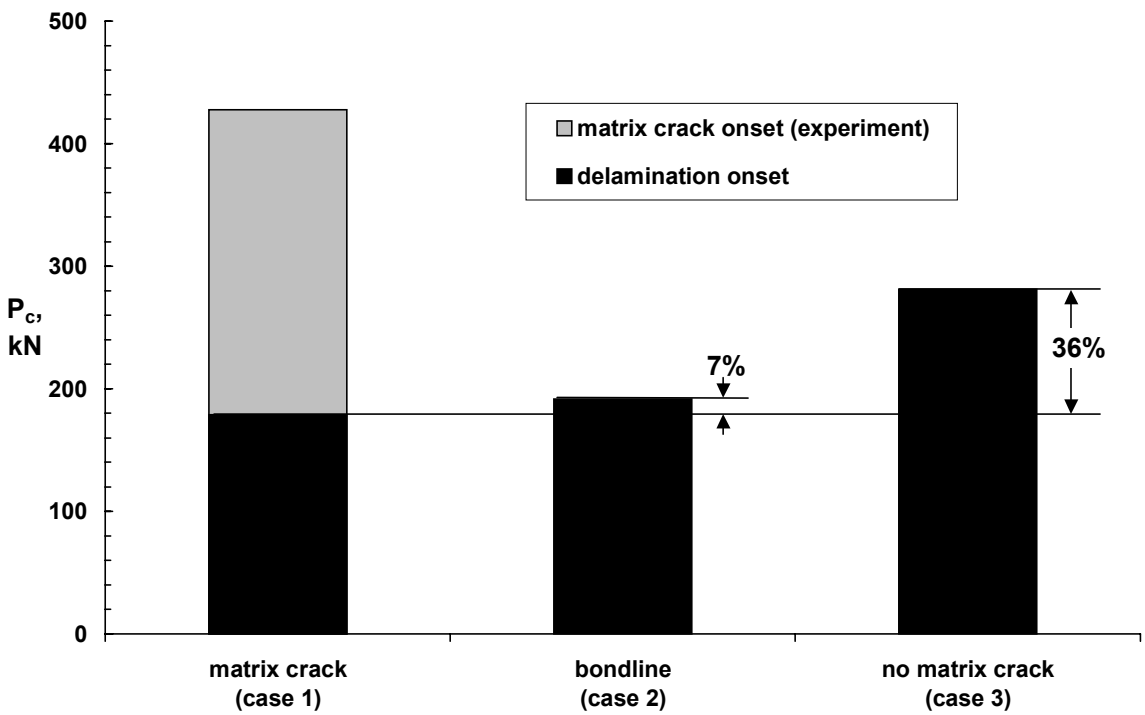

Figure 12. Critical load P_c for bending loading condition.

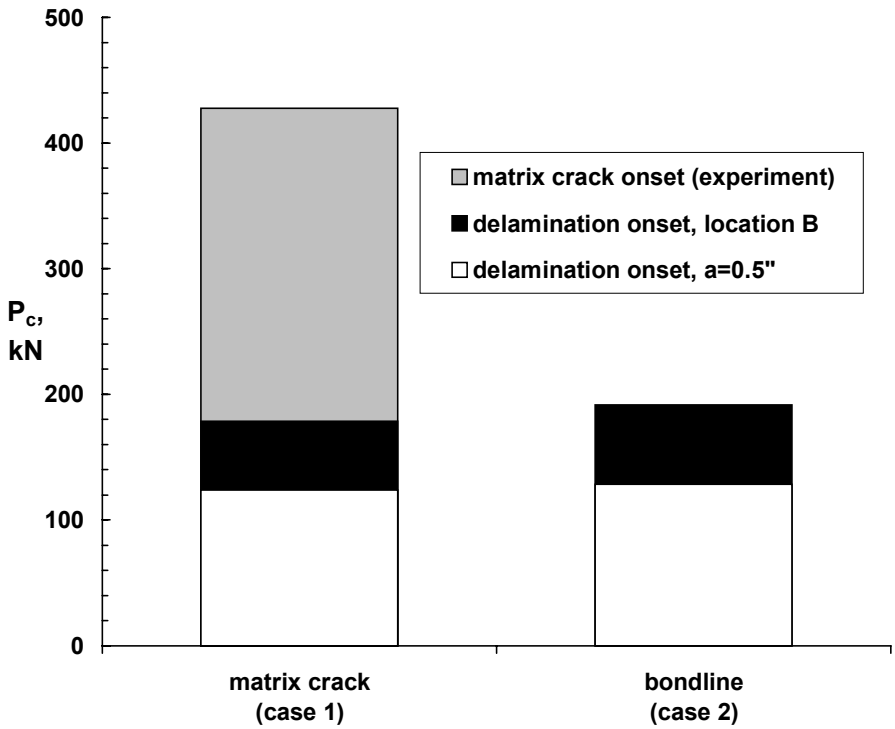

Figure 13. Critical load P_c for an assumed flaw of 12.7 mm (0.5”) for bending loading condition.